RSC Advances

ROYAL SOCIETY OF CHEMISTRY

www.rsc.org/advances

Functionalized mesoporous carbon nanoparticles for targeted chemo-photothermal therapy of cancer cells under near-infrared irradiation

Guiju Xu[a,b], *Shengju Liu*[a,b], *Huan Niu*[a,b], *Wenping Lv*[a], *Ren'an Wu*[a,*]

[a] CAS Key Laboratory of Separation Science for Analytical Chemistry, National Chromatographic R & A Center, Dalian Institute of Chemical Physics, Chinese Academy of Sciences (CAS), Dalian 116023, China

[b] The University of Chinese Academy of Sciences, Beijing 100049, China

***The corresponding Author Footnote:**

Dr. Ren'an Wu (wurenan@dicp.ac.cn)
Professor of Chemistry
Tel: +0086-411-84379828
Fax: +0086-411-84379617

Abstract

Chemo-photothermal therapy with the combination of chemotherapy and photothermal therapy has emerged as a promising anticancer treatment for its synergistic effects. In this work, the functionalized mesoporous carbon nanoparticles (FA/PEI/O-MCN) were constructed by modifying the mesoporous carbon nanoparticles (MCN) with polyethylenimine (PEI) and folic acid (FA) for the targeted chemo-photothermal therapy. The FA/PEI/O-MCN exhibited strong light absorption and high photothermal conversion efficiency in the near-infrared (NIR) region due to the graphite structure of MCN. Meanwhile, FA/PEI/O-MCN displayed high drug loading capacity using doxorubicin hydrochloride (DOX) as a model drug. Flow cytometry analysis and competitive binding experiments verified that the FA modification could significantly enhance the uptake of FA/PEI/O-MCN by HeLa cells with folate receptors (FR) over-expressing. Comparing with chemotherapy or photothermal therapy alone, the DOX-loaded FA/PEI/O-MCN demonstrated the synergistic effects and resulted in the higher therapeutic efficacy. We believe that the FA/PEI/O-MCN could be applied as an efficient chemo-photothermal platform to realize the targeted synergistic therapy.

Keywords: chemo-photothermal therapy, mesoporous carbon, near-infrared, DOX, synergistic effects

Introduction

Photothermal therapy is a physical treatment, in which light is converted into cytotoxic heat to destroy tumor cells.[1] In terms of light source, the use of near-infrared (NIR) light is highly desirable since NIR light (wavelength 700-1100 nm) is noninvasive for normal tissues and possesses long penetration depth.[2] As the efficacy of photothermal therapy could be enhanced by nanomaterials, a series of NIR-resonant nanomaterials such as metal nanomaterials (e.g., gold nanorods,[3] gold nanocages,[4 5] gold nanoshells,[6] gold nanostars[7] and Pd nanosheets[8]) and carbon nanomaterials (e.g., carbon nanotubes,[9 10 11] carbon nanohorns,[12 13] graphene oxide[14] and graphene shell[15 16]) have been developed for the photothermal treatment of cancer cells. To improve the therapeutic efficacy, chemo-photothermal therapy with the combination of photothermal therapy and chemotherapy has been developed, which can induce the synergistic effects by delivering the cytotoxic heat and drugs to the tumor sites simultaneously and locally.[17] Additionally, chemo-photothermal therapy can lower the drug dosage requirements and minimize systemic side-effects of chemotherapeutic agents, since not only the cytotoxicity of chemotherapeutic agents can be enhanced at elevated temperatures[18] but also photothermal therapy can sensitize the tumor to chemotherapeutic agents.[10]

To date, different types of NIR-resonant nanomaterials have been developed for chemo-photothermal therapy. The graphitic structure (such as carbon nanotubes and graphene etc.) could provide the hydrophobic surface for drug-loading and also endow the optical absorption in near-infrared regions. Previously, we have utilized carbon nanotube to serve as the NIR-triggered drug-delivery nanosystem to overcome the drug-resistance of human leukemia cancer cells due to its efficient drug loading capacity as well as NIR absorption.[19] To combine drug delivery and NIR photothermal therapy into one system, nanoscale graphene oxide with high optical absorbance in NIR region has been used in chemo-photothermal therapy.[20 21] The surface modification of graphene with stabilizing agents such as PEG-lipid and PVP were applied, with the view to maintain the stability of graphene in physiological solutions.[22 23] On the other hand, metal-based NIR-resonant nanomaterials also have

the potential to combine drug delivery and NIR-resonant into one system, such as gold nanostars.[24] However, the improvement of drug-loading capacity usually required since the nonporous structure of most metal-based NIR-resonant nanomaterials. Besides, the NIR absorption band will be disappeared for gold nanorods exposed to NIR laser because of the transformation tendency from gold nanorod to gold nanosphere.[25] So, the hybrid nanocomposites with the integration of NIR-resonant nanomaterials (e.g., gold nanorods,[26 27 28 29] gold nanocages,[30] and Pd nanosheets[31]) and mesoporous silica were developed. In these hybrid nanocomposites, the drugs are stored in nanopores of mesoporous materials, and the heat is generated by light on the NIR-resonant nanomaterials. The mesoporous structures not only improve the drug loading performance for the metal-based NIR-resonant nanomaterials but also provide the opportunity to archive the controlled release of drugs by installing nanovalves on mesopores.[32] Despite so much progress has been made for the NIR-resonant nanomaterials applied in chemo-photothermal therapy, seeking for a new platform possessing inherent high drug-loading capacity, good water-solubility and efficient NIR photon-to-heat conversion is still meaningful for chemo-photothermal therapy.

Mesoporous carbon prepared by the hard or soft templating synthetic methods have received significant attention owing to large surface area, tunable pore size, good biocompatibility and well-defined surface properties. Due to the strong hydrophobicity of the internal surface of mesoporous carbon materials, we have demonstrated the highly efficient loading of endogenous peptides from human serum [33]and N-linked glycans from glycoprotein by ordered mesoporous carbon.[34] Matching with the targeted tumor therapy via the enhanced permeability and retention (EPR) effect, nanosized mesoporous carbon materials have emerged potentials in drug delivery systems (DDS).[35 36 37] So far, research attention on mesoporous carbon nanoparticles (MCN) has only been paid on drug-loading properties since the hydrophobicity and large surface area,[38 39 40] the investigation of using MCN as NIR-resonant nanomaterials combining with the drug-loading for chemo-photothermal therapy has not been reported, to the best of our knowledge. In

this work, a MCN-based nanosystem has been developed to serve as an integrated system for combined drug delivery and NIR photothermal therapy. The functionalized MCN (FA/PEI/O-MCN) were constructed via the modification of the pristine MCN with polyethylenimine (PEI) and cancer-cell-specific ligand folic acid (FA). FA were incorporated for specific recognition of cancer cells and enhance the cellular uptake of FA/PEI/O-MCN.[41] As expected, the obtained FA/PEI/O-MCN exhibited strong absorption of NIR light and efficient photothermal conversion, superior to that of reduced graphene oxide. Doxorubicin hydrochloride (DOX) was used as a model anticancer drug since DOX can emit fluorescence, allowing for study of cellular uptake using flow cytometry. The inherent mesoporous structure of FA/PEI/O-MCN was desirable for efficient loading of DOX. Flow cytometry analysis and competitive binding experiments demonstrated that the FA modification could facilitate the internalization of FA/PEI/O-MCN into HeLa cells with over-expressed folate receptor (FR). The combined NIR photothermal therapy and chemotherapy with the DOX-loaded FA/PEI/O-MCN complex showed excellent efficacy for the treatment of HeLa cells, superior to NIR photothermal therapy or chemotherapy alone. In summary, FA/PEI/O-MCN could efficiently combine NIR-induced hyperthermia, drug delivery and receptor-specific targeting into one system for targeted chemo-photothermal therapy, as illustrated in Figure 1.

2. Experimental Section

2.1. Materials and apparatus

Triblock copolymer Pluronic F127 and folic acid were purchased from Sigma–Aldrich (St. Louis, MO). Formaldehyde, phenol, sodium hydroxide and sodium borohydride were purchased from Sinopharm Chemical Reagent Co. Ltd. (Shanghai, China). N-hydroxysuccinimide (NHS), 1-[3-(dimethylamino) propyl]-3-ethylcarbodiimide hydrochloride (EDC) and branched polyethylenimine (PEI, MW=600) were purchased from Alfa Aesar (Ward Hill, MA). 2-(4-morpholino) Ethanesulfonic acid was purchased from Aladdin (Shanghai, China). Polyvinylpyrrolidone (PVP, MW=58000) were purchased from Bailingwei Chemical

Regant Co.Ltd. (Shanghai, China). Doxorubicin hydrochloride (DOX) was purchased from Meilun Biology Technology Co. Ltd. (Dalian, China). RPMI-1640 cell culturing medium and penicillin/streptomycin solution (100×) were purchased from Gibco Invitrogen Corporation (Carlsbad, CA). Cell Counting Kit-8 was purchased from Dojindo laboratory (Kumamoto, Japan). The LDH Assay Kit was acquired from the Beyotime Institute of Biotechnology (Haimeng, China). Sulfuric acid (H_2SO_4), nitric acid (HNO_3), concentrated ammonia and ethanol were of analytical grade. Deionized water was purified with a Milli-Q water system (Millipore, USA).

Transmission electron microscopy (TEM) measurements were carried out on a JEM-2000 EX (JEOL) microscope operated at 120 kV. UV-Vis-NIR spectra were measured on a Double Beam UV-Vis spectrophotometer (UV-8000S) (Metash) at a wavelength of 190−1100 nm. Dynamic light scattering (DLS) and zeta potential measurements were made on a Zetasizer nano ZS (ZEN3600) instrument (Malvern). Fourier transform infrared (FTIR) spectra were taken in KBr disks on a Tensor 27 spectrometer (Bruker). Nitrogen sorption isotherms were measured at 77 K with BK122W (JWGB). Raman spectra were taken at room temperature on a Renishaw invia spectrometer with an argon-ion laser at an excitation wavelength of 514 nm. Flow cytometry analysis were performed with a FACS Vantage SE flow cytometer (BD).

2.2. Experimental details

2.2.1 Synthesis of mesoporous carbon nanoparticles (named as MCN). The MCN were synthesized according to the low-concentration hydrothermal route.[37] Briefly, phenol (0.6 g), formalin aqueous solution (2.1 mL, 37 wt%) and NaOH aqueous solution (15 mL, 0.1 M) were mixed and stirred at 70 °C for 0.5 h to obtain the phenolic resols. After the addition of triblock copolymer Pluronic F127 (0.96 g) dissolved in H_2O (15 mL), the mixture was stirred at 340 rpm at 66 °C for 2 h. Then, water (50 mL) was added, and the solution was further reacted for 16-18h. After that, the obtained solution was diluted by water in a volume ratio of one to three, transferred into an autoclave and heated at 130 °C for 24 h. The products were collected by centrifugation and washed with water for three times and dried under

vacuum. The resulting powders were then heated at 700 °C for 3 h in nitrogen flow to remove the template.

2.2.2 Oxidization of MCN (named as O-MCN). The obtained MCN were added to a mixed solution of the concentrated sulfuric acid (98%) and concentrated nitric acid (70%) with the ratio of 3:1 (v/v), and sonicated for 4 h at 35-40 °C. The oxidized MCN (O-MCN) were collected by centrifugation and washed with water till the pH neutral of the washed water. The obtained O-MCN were finally dried under vacuum overnight.

2.2.3 Procedures for PEI functionalization of O-MCN (named as PEI/O-MCN). The grafting of PEI onto O-MCN was carried out by covalently bonding polyethylenimine (PEI, MW=600) onto O-MCN via the diimide-activated amidation. Briefly, O-MCN (80 mg) were first dissolved in a 40 mL aqueous buffer solution of 2-(4-morpholino) ethanesulfonic acid (MES) (50 mM, pH =6.0), and then activated with stirring gently at 25 °C for 0.5 h after the addition of EDC (190 mg, 1 mmol) and NHS (287 mg, 2.5 mmol). After that, the PEI (600 mg,1 mmol) dispersed in the MES solution (5 mL) was added to the activated O-MCN solution and stirred for another 24 h at 25 °C. Finally, the excess EDC, NHS and PEI were removed by washing the materials repeatedly with water for several times. At last, the PEI grafted O-MCN (PEI/O-MCN) were dried under vacuum for 12 h at 60 ˚C.

2.2.4 Synthesis of folic-acid-conjugated PEI/O-MCN (named as FA/PEI/O-MCN). Firstly, folic acid (220 mg, 0.5 mmol), 1-(3-dimethylaminopropyl)-3-ethylcarbodiimide hydrochloride (EDC, 90 mg, 0.5 mmol) and N-hydroxysuccinimide (NHS, 145 mg, 1.25mmol) were mixed in DMSO (25 mL) and stirred gently at 25 ˚C for 0.5 h. Then, the PEI/O-MCN (50 mg) pre-dispersed in DMSO was added and stirred at room temperature for 24 h. The resulting solids were centrifuged and washed with DMSO, water, and ethanol, successively. The obtained products (FA/PEI/O-MCN) were then dried under vacuum at 60 °C for 12 h.

2.2.5 Synthesis of PVP-modified reduced graphene oxide (named as rGO_{pvp}). Graphene oxide (GO) was purchased from XFnano (Nanjing, China). The reduced

graphene oxide (rGO) was reduced from GO with sodium borohydride using a method reported elsewhere.[42] Briefly, 30 mg GO was first immersed in a diluted ammonia solution to form a solution of GO with the concentration of 1 mg/mL (pH 11.8-12.8) under a 30 min sonication. After the following addition of 60 mg sodium borohydride into this suspension, the reduction process of the GO was performed by stirring and refluxing for 12 h. The resulting reduced graphene oxide (rGO) was further modified by polyvinylpyrrolidone (PVP) to prepare a stable water suspension following a literature protocol [43].

2.2.6 DOX Loading and Loading Yield Measurement. 1 mg of FA/PEI/O-MCN nanoparticles were suspended in 5 mL of DOX aqueous solution (180 μg/mL) with pH values of 9, 7.4 and 5.5, respectively, in Tris-HCl, phosphate and acetate buffers. After 24 h stirring under dark, the FA/PEI/O-MCN nanoparticles were collected by centrifugation, and carefully washed with the corresponding buffer till the supernatant turned colourless. The amount of DOX loaded on FA/PEI/O-MCN was estimated by monitoring the concentrations of DOX in the initial solution and the supernatant by UV-Vis spectrometry at 480 nm.

2.2.7 DOX Release. To examine the release of DOX from FA/PEI/O-MCN, the DOX-loaded FA/PEI/O-MCN nanoparticles were first dispersed in 5 mL buffer at various pH (5.5 and 7.4) in a 20 mL transparent glass bottle. Then, the bottle was placed into a shaker and shook for a certain time under dark with 150 rpm at 37 °C. At predetermined time intervals, the nanomaterials solution was centrifuged (11,000 rpm, 10 min), and the supernatant was withdrawn. After the samples were redispersed in 5 mL fresh buffer and irradiated with NIR laser centered at 808 nm at an output power of 15 W/cm^2 for 5 min under magnetic stirring, the nanomaterials solution was centrifuged (11,000 rpm, 10 min) and supernatant was withdrawn. The concentrations of DOX in the supernatant before and after NIR laser irradiation were analyzed by UV-Vis spectrometry. The release behavior was also performed without NIR laser irradiation at different pH values.

2.2.8 CCK8 and the LDH activity assay for measuring cell viability. The impact of FA/PEI/O-MCN on cell proliferation was determined by CCK8 and LDH activity

assays. Unless otherwise stated, HeLa cells (a human cervical carcinoma cell line) were cultured in complete culture media (RPMI 1640 supplemented with 10% bovine serum and 0.1% penicillin/streptomycin) in 5% CO_2 atmosphere at 37 °C in a humidified incubator. For cell viability measurements, HeLa cells were plated into 96-well plates and cultured until a confluency of 80% was reached. HeLa cells were treated with FA/PEI/O-MCN at different concentrations in culture media. Cells cultured in blank composites medium were taken as the control. After 12 h, 24 h and 48 h, the viability of HeLa cells were determined by the CCK8 assay and LDH activity assay, according to the manufacturer suggested procedures.

2.2.9 **Assessment of targeting ability of FA/PEI/O-MCN.** For optical microscope images observation, HeLa cells were pre-grown in 6-well culture plates using folate-deficient RPMI 1640 medium (named as folate-free medium) and cultured until a confluency of 80% was reached. The cell medium was removed, and then cells were incubated with fresh cell medium containing 25 μg/mL of FA/PEI/O-MCN for 12 h. For folic acid competition experiments, HeLa cells were cultured in the medium containing 3mM free folic acid (named as folate medium). After removal the cells medium, the cells were rinsed and viewed live with the Olympus CKX 41 microscope.

For flow cytometry analysis, HeLa cells were pre-grown in 6-well culture plates using folate-deficient RPMI 1640 medium (named as folate-free medium) and cultured until a confluency of 80% was reached. Next, the DOX -loaded PEI/O-MCN or FA/PEI/O-MCN was added at a concentration of 25 μg/mL in the same medium and incubated for 2 h. Then the cells were washed with PBS buffer for 3 times and collected. The measurement of intracellular DOX levels was fulfilled by a FACS Vantage SE flow cytometer from BD (Franklin Lakes, NJ).

The influence of target unit on the efficiency of cell killing by FA/PEI/O-MCN combined with NIR laser irradiation was investigated. The cells cultured in different medium (folate medium and folate-free medium) were treated with the same concentration of FA/PEI/O-MCN for 8 h. Then, the cell culture was washed three times with PBS and replaced by 100 μL fresh culture media. After that, the cells on

plate were exposed to 808 nm laser irradiation (15 W/cm^2 for 5 min per treatment, three treatments), and incubated for another 12 h at 37 °C. Cell viability was measured by the CCK8 assay.

2.2.10 Chemo-photothermal therapy of HeLa Cells. HeLa cells seeded on 96-well plates with a confluency of 80 % were treated FA/PEI/O-MCN and DOX-loaded FA/PEI/O-MCN at various concentrations for 8 h. Cellular unbound nanoparticles were removed by rinsing with PBS. After the addition of fresh culture media into wells, the cells were irradiated by 808 nm laser (15 W/cm^2 for 5 min per treatment, three treatments) for photothermal and chemo-photothermal treatments, respectively. For chemotherapy alone, the cells were not exposed to NIR irradiation. Afterwards, the cells were incubated at 37 °C for a further 12 h. Cell viability was measured by the CCK8 assay. The data reported represented the means of triplicate measurements.

To monitor the changes of temperature in the culture chamber arising from NIR laser irradiation, HeLa cells seeded on 96-well plates with a confluency of 80 % were first incubated with FA/PEI/O-MCN at various concentrations for 8 h. Then, cellular unbound nanoparticles were removed by rinsing with PBS. After the addition of fresh culture media into wells, the cells were irradiated by 808 nm laser (15 W/cm^2 for 5 min). The temperature changes were measured by a Fluke thermometer with a thermocouple suspended in the growth medium.

3. Results and discussion

3.1 Preparation and characterization of FA/PEI/O-MCN

The synthesis of FA/PEI/O-MCN is shown in Figure 1. Firstly, the mesoporous carbon nanoparticles (MCN) were synthesized according to the low-concentration hydrothermal route.[37] To further improve the water-solubility of the as-synthesized MCN, MCN were oxidized by a mixture of the concentrated HNO_3 and the concentrated H_2SO_4 (v/v, 1/3) with bath sonication (denoted as O-MCN). For the sake of subsequent conjugation of folic acid, the low-molecular-weight and hyper branched polyethylenimine (PEI) with high surface concentration of amino-groups was covalently linked on the surface of O-MCN through carbodiimide coupling (denoted as PEI/O-MCN). Folic acid (FA) was conjugated through a covalent amide

linkage between the carboxyl group in FA and the amino group in the PEI chain (denoted as FA/PEI/O-MCN) to endow the MCN with the targeting ability.

The shape and porous structure were characterized by Transmission electron microscopy (TEM). As shown in Figure 2A, the pristine MCN are roughly spherical in shape with a diameter of ca. 100 nm. TEM images showed that there were no obvious changes in the mesoporous structure of O-MCN before and after the conjugation with PEI (Figure 2A-2 and 2A-3). The hydrodynamic diameter of the functionalized MCN (FA/PEI/O-MCN) was measured by the dynamic light scattering (DLS) analysis with nanoparticles dispersed in phosphate buffered saline (PBS, pH=7.4) by sonication. The average hydrodynamic diameter of the FA/PEI/O-MCN was about 120 nm (Figure 2B), close to the particle size observed by TEM. The polydispersity index (PDI), reflecting the dispersity of nanoparticles, was 0.172 which indicated the monodisperse distribution of the FA/PEI/O-MCN. The surface area and pore size distribution were 517 m^2/g and 3.2 nm for the O-MCN, and 312 m^2/g and 2.6 nm for the FA/PEI/O-MCN, as characterized by N_2 adsorption–desorption at 77 K (Figure 2D). The structural information of the pristine and functionalized MCN was investigated by Raman spectroscopy. As shown in Figure 2C, a graphite-like band (G-band) at ~1600 cm^{-1} and a disorder-induced band (D-band) at ~1380 cm^{-1} were observed. The D-band was used to characterize the amorphous or disordered carbon. The G-band was related to the vibration of sp^2-hybridized carbon atoms, which verified the presence of graphitic domains.[44] The existence of the G-band in all samples suggests that the well defined graphitic domains are indeed developed. It has been reported that the G/D-band ratio is nearly proportional to graphitization degree.[45] As observed, the ratios of G/D-band are 1.41, 1.38, and 1.33 for samples MCN, O-MCN and FA/PEI/O-MCN, respectively. The almost unchanged G/D-band ratio for the pristine and functionalized MCN suggested that the graphitic structure is well preserved.

To evaluate the functionalization of the MCN-based vectors by branched PEI and folic acid, the resulting products were characterized by FTIR spectroscopy, with the data presented in Figure 3A. A band of O-H stretching vibrations due to the

existence of surface hydroxyl groups or chemisorbed water was observed in all the recorded spectra in the range of 3600-3200 cm^{-1}.[46] The bands at 3448 and 1723 cm^{-1}, representing the typical stretching vibrations of O-H and C=O attributed to the formation of carboxylic structures were observed in the IR spectrum of O-MCN. The band at 1587 cm^{-1} was corresponding to the aromatic ring stretching coupled to highly conjugated keto groups. The band at 1250 cm^{-1} might be attributed to C–O–C vibrations.[47] Two additional bands were observed at 1400 and 750 cm^{-1} in the IR spectra of PEI/O-MCN and FA/PEI/O-MCN. The bands at 1400 cm^{-1} could be assigned to the stretching vibrations of C-N. The new intense band at 750 cm^{-1} was attributed to the $–NH_2$ vibrations.[48] The FTIR technique was insufficient to distinguish FA signals in FA/PEI/O-MCN from those in PEI/O-MCN. The UV-Vis spectrum was recorded to further confirm the successful conjugation of FA on MCN.[49] We detected the UV-Vis-NIR spectra of PEI/O-MCN@PEI and FA/PEI/O-MCN with the same concentration in PBS. Then spectra subtraction was applied by subtracting the spectrum of PEI/O-MCN from the spectrum of FA/PEI/O-MCN, and the obtained spectrum was named as residual spectrum. As shown in Figure 3B, the conjugation of FA on the nanospheres was demonstrated from the spectrum of the FA/PEI/O-MCN and residual spectrum, which showed the characteristic absorption peaks (280 nm) of FA.[50] Meanwhile, the UV-Vis-NIR spectrum indicated that the FA/PEI/O-MCN exhibited broad absorption from the UV to the NIR region, which was similar to carbon nanotubes and graphene reported in previous studies.[11 14]

Moreover, the surface modifications on MCN could be reflected by the change of the zeta potential. Figure 4 showed the zeta potential of functionalized MCN at phosphate buffered saline (PBS, pH=7.4). As the existence of hydroxyl and carboxyl groups on O-MCN, the zeta potential of O-MCN was -39.7 mV. After grafting with PEI, the zeta potential of PEI/O-MCN was increased to +2.5 mV, which indicated the existence of a great amount of amino groups. Due to the successful functionalization with FA, the zeta potential of FA/PEI/O-MCN was decreased to -16.1 mV.

3.2 Photothermal effect of FA/PEI/O-MCN

To test the feasibility of FA/PEI/O-MCN as photothermal agents, we chose an 808 nm laser to evaluate the photothermal conversion capability of FA/PEI/O-MCN. The FA/PEI/O-MCN were dispersed in phosphate buffered saline (PBS, pH=7.4) at concentrations ranging from 6.25 to 75 μg/mL, and irradiated with an 808 nm laser at a power density of 15 W/cm^2 for 5 min. PBS was used as a negative control. As illustrated in Figure 5A, no obvious temperature increase was observed for PBS alone after 5 min NIR laser irradiation. In contrast, the temperature was increased with irradiation time for all FA/PEI/O-MCN solutions. Furthermore, temperature evolution of FA/PEI/O-MCN at increasing concentrations from 6.25 to 75 μg/mL revealed an obvious concentration-dependent temperature increase under NIR laser irradiation. It was vital that no sedimentation of the FA/PEI/O-MCN suspension was observed even for temperature higher than 37 °C, and the heating rate was not affected by the influence of NIR irradiation times. The ratios of G/D-band for the FA/PEI/O-MCN were 1.30 and 1.33 after and before the NIR laser irradiation, which confirmed that the FA/PEI/O-MCN not only could convert NIR photon energy into thermal energy but also were thermostable. The existence of graphitic structure on FA/PEI/O-MCN may be related to explain the infrared-absorption mechanism in functionalized MCN.[15 51]

As the reduced graphene oxide exhibited excellent NIR absorbance and photothermal heating effect,[52 53] the comparison of the photothermal efficiency between the FA/PEI/O-MCN and the reduced graphene oxide was carried out. To prevent reduced graphene oxide aggregation in aqueous dispersions, polyvinylpyrrolidone (PVP) has to be introduced as stabilizing agents. Comparing the UV-Vis-NIR spectra of FA/PEI/O-MCN and rGO_{pvp} with the concentration of 50 μg/mL, we found that FA/PEI/O-MCN exhibited stronger absorbance than rGO_{pvp} at 808 nm (Figure 5B, inset). A series of PVP-modified reduced graphene oxide (rGO_{pvp}) solutions with different concentrations were irradiated with an 808 nm laser at a power density of 15 W/cm^2 for 2.5 min. The rGO_{pvp} showed a concentration-dependent temperature increase in response to the NIR laser irradiation (Figure 5B). It was observed that heat could be generated more efficiently by

FA/PEI/O-MCN than rGO_{pvp} with the same concentration. These data indicated that the photothermal sensitivity of FA/PEI/O-MCN was superior to that of rGO_{pvp}. The excellent NIR absorption and photothermal conversion efficiency of FA/PEI/O-MCN prompted us to evaluate their feasibility as NIR-resonant materials for cancer therapy.

3.3 Doxorubicin loading and release properties of FA/PEI/O-MCN

The structural features of FA/PEI/O-MCN are highly desirable for drug delivery because of the large specific surface area and mesopores. To evaluate the loading performance of FA/PEI/O-MCN for drugs, doxorubicin hydrochloride (DOX), an aromatic anticancer agent, was used as the model drug, and the FA/PEI/O-MCN were mixed with DOX at varied pH for drug loading. Figure 6A showed that the loading efficiency of DOX on FA/PEI/O-MCN increased with an increase in the pH value. Speaking concretely, the loading amount of DOX on FA/PEI/O-MCN was 100 μg/mg at pH 5.5, 520 μg/mg at pH 7.4, and 750 μg/mg at pH 9.0. The pH-dependent DOX loading on FA/PEI/O-MCN was similar to that with carbon nanotubes and graphene oxide.[54 55] The existence of hydrophobic interior surface and graphite structure of the FA/PEI/O-MCN and the pH-dependant solubility of DOX made this phenomenon reasonable.[54] That is the decreased hydrophilicity of DOX at a higher pH and the resultant enhanced hydrophobic interaction between DOX and FA/PEI/O-MCN. To be convenient, the DOX-loaded FA/PEI/O-MCN refers to the products of loading at pH values of 7.4 in the following descriptions unless specified otherwise. Comparing the loading capacity of FA/PEI/O-MCN and O-MCN (Figure 6A), the conjugation of PEI and FA on the FA/PEI/O-MCN exhibited negligible influence on the loaded amount of DOX, suggesting that the subsequent modification did not compromise the loading efficiency of DOX.

In order to mimic the approximate neutral environment of blood circulation system and the acidic condition in cellular endosome, the release profile of DOX from FA/PEI/O-MCN was examined at pH 7.4 and 5.5, respectively. As shown in Figure 6B, the cumulative release of DOX from FA/PEI/O-MCN demonstrated a much rapid release of DOX at acidic condition (6.8 % at pH 5.5) than the neutral condition (1.2% at pH 7.4). The observed higher release rate of DOX from

FA/PEI/O-MCN at acidic condition than basic condition could be attributed to the increased hydrophilicity of DOX at acidic condition, which weakened the π-π stacking and hydrophobic interactions between DOX and FA/PEI/O-MCN and made the dissociation of DOX from FA/PEI/O-MCN easier.

To examine whether the NIR laser irradiation would affect the release behavior of DOX from FA/PEI/O-MCN, the release kinetics of DOX was also investigated with the assistance of NIR laser irradiation. As shown in Figure 6B inset, the release profile of DOX at acidic conditions (pH 5.5) indicated that no burst release of drugs occurred in the absence of NIR laser irradiation. In contrast, a sudden release of DOX from FA/PEI/O-MCN could be observed, once the NIR light switched on. As revealed by the bar chart in Figure 6B, the NIR laser irradiation could increase the release of DOX from FA/PEI/O-MCN regardless of the acidic or basic conditions. In detail, the release rate of DOX reached 3.8% at pH 7.4 and 15.7% at pH 5.5 within 9 h. The accelerated release of DOX from FA/PEI/O-MCN with NIR laser irradiation could be ascribed to the laser-converted heat which weakened the interactions between DOX and FA/PEI/O-MCN.[56]

3.5 In vitro cytotoxicity of FA/PEI/O-MCN

The cytotoxicity of FA/PEI/O-MCN to HeLa cells was investigated by Cell Counting Kit-8 (CCK8) assay and lactate dehydrogenase (LDH) Assay. It could be seen from Figure 7 that the FA/PEI/O-MCN showed no obvious cytotoxicity to the HeLa cells at concentrations of 10–75 μg/mL with incubation time of 12 h, 24 h and 48 h. Both in vitro CCK8 and LDH assays clearly indicated the FA/PEI/O-MCN showed low cytotoxicity and good biocompatibility.

3.6 Targeted ability of FA/PEI/O-MCN

The flow cytometry analysis was used to study the cellular uptake efficiency of FA/PEI/O-MCN in FR-positive HeLa cells. The HeLa cells were incubated with DOX-loaded FA/PEI/O-MCN and DOX-loaded PEI/O-MCN for 2 h at 37 °C at a dose of 25 μg/mL, respectively. As shown in Figure 8A, much greater fluorescence intensity of DOX was observed in HeLa cells treated with DOX-loaded FA/PEI/O-MCN than that treated with DOX-loaded PEI/O-MCN. Because the only

difference between these two sets of nanocarriers was the FA functionalization, this proved that the increased internalization of FA/PEI/O-MCN into HeLa cells is due to FA functionalization.

The FR blocking experiment further evidenced the highly specific FR targeting by FA/PEI/O-MCN. [57] As discussed previously, the existence of free FA had negative impacts on the expression of folate receptors on the surface of HeLa cells.[58] FA/PEI/O-MCN was placed in two different media: (1) folate-free medium (the cells in this medium are considered as high folate expressing HeLa cells); (2) folate medium (the cells in this medium are considered as folate-receptor blocking HeLa cells, because it contains 3 mM FA). The semi-qualitative indication of the interactions between FA/PEI/O-MCN and cells via an optical microscopy could be observed based on the intensity of dark signal (from FA/PEI/O-MCN) and its association with cells.[55] Figure 8B showed that the FA/PEI/O-MCN dispersed in folate-free medium were remarkably internalized and existed as black granules in the cells. While FA/PEI/O-MCN with the same concentration (25 μg/mL) dispersed in folate medium were internalized with a lower efficiency by HeLa cells. This result demonstrated that with free FA serving as a competitive inhibitor, the uptake amount of FA/PEI/O-MCN was reduced due to loss of availability of the folate receptors on the cancer cell surface. This in turn verified that the FA functionalized FA/PEI/O-MCN could target HeLa cells via the folate receptors.

In addition to the optical microscope images described above, we tested the viability of HeLa cells incubated with FA/PEI/O-MCN dispersed in different medium under NIR laser irradiation. HeLa cells cultured in two different medium (folate medium and folate-free medium) were incubated with FA/PEI/O-MCN (25 μg/mL) for 8 h, washed to remove nanoparticles, and then exposed to an 808 nm laser at a power density of 15 W/cm^2 for 5 min. 50% of HeLa cells treated by FA/PEI/O-MCN dispersed in folate-free medium were killed after NIR laser irradiation (Figure 8C), while FA/PEI/O-MCN dispersed in folate medium treated cells showed much less cell death after exposure to the NIR laser. As the aforementioned, the photothermal effect was concentration dependent. For free folate in the culture media competitively

bound to the folate receptors on the cell surface, the uptake amount of FA/PEI/O-MCN was negligible, and thereby insufficient heat was transformed into cells, which accounted for their high survival of HeLa cells under NIR laser irradiation. The selective thermal ablation of HeLa cells using FA/PEI/O-MCN with the assistance of NIR laser irradiation further confirmed the targeted uptake of FA/PEI/O-MCN.

3.7 Chemo-photothermal therapy based on FA/PEI/O-MCN

To investigate the efficiency of NIR-photothermal therapy based on FA/PEI/O-MCN, HeLa cells were incubated with FA/PEI/O-MCN at concentrations of 6.25, 12.5 and 25 μg/mL for 8 h. The cell viabilities were measured by cell-counting kit-8 (CCK8) assay with or without NIR laser irradiation. As shown in Figure 9A, FA/PEI/O-MCN produced negligible toxicity to HeLa cells in the absence of NIR laser irradiation. In contrast, the viability showed a dramatic dose-dependent decrease for cells incubated with FA/PEI/O-MCN and exposed to NIR laser. It was reported that the temperature higher than 42 or 43 °C would begin to induce cellular death.[56] To determine the cancer cells death induced by the temperature increase of FA/PEI/O-MCN under NIR laser irradiation, a thermocouple was suspended in the growth medium of the culture chamber to monitor the change of temperature during the process of NIR laser irradiation. For the control experiment, the cells were cultured in the medium with the absence of FA/PEI/O-MCN. As shown in Figure 9B, the increase of temperature depended upon the concentration of FA/PEI/O-MCN. The ΔT for control cells, which did not contact any FA/PEI/O-MCN, was merely 3.8 °C for 5 min irradiation. In contrast, for cells cultured with 50 μg/mL FA/PEI/O-MCN, the ΔT value was elevated to 39.9 °C under 5 min exposure to NIR laser. The significant increase of temperature induced by NIR laser irradiation demonstrated that the FA/PEI/O-MCN would be a highly efficacious platform to perform the photothermal treatment.

To evaluate the efficiency of FA/PEI/O-MCN for targeted chemo-photothermal therapy, HeLa cells were incubated with different concentrations of DOX-loaded FA/PEI/O-MCN and FA/PEI/O-MCN (6.25, 12.5 and 25 μg/mL) for 8 h and exposed

to NIR light. Figure 9A showed the cytotoxicity of these treatments increased with the increase of their concentrations. When the cells were treated with FA/PEI/O-MCN (25 μg/mL) and exposed to NIR laser irradiation, 50 % of HeLa cells were killed. The inhibition rate of DOX-loaded FA/PEI/O-MCN (25 μg/mL, with an equivalent of 13 μg/mL DOX) in the absence of NIR laser irradiation was 64%. Upon NIR laser irradiation, the inhibition rate of DOX-loaded FA/PEI/O-MCN was increased to 74%. Comparing the cell killing efficiency, it was obvious that the combination of chemotherapy and NIR-photothermal therapy based on DOX-loaded FA/PEI/O-MCN was superior to the chemotherapy or photothermal therapy alone. It demonstrated that DOX-loaded FA/PEI/O-MCN under NIR laser irradiation could selectively carry heat and drug to cancer cells and significantly enhance the therapeutic efficacy of chemo-photothermal.

Conclusion

In summary, the efficient nanocarriers based on the functionalized mesoporous carbon nanoparticles (FA/PEI/O-MCN) were designed to perform the drug delivery and NIR photon-to-heat conversion for the chemo-photothermal synergistic therapy of HeLa cells. The FA/PEI/O-MCN showed promising features of the ease of synthesis and functionalization, good water-solubility and stability in physiological solutions, as well as their biocompatibility. The inherent mesoporous structure made FA/PEI/O-MCN a favorable drug delivery nanocarriers for chemotherapy. The efficient NIR photon-to-heat conversion and good thermal stability made FA/PEI/O-MCN an ideal platform for NIR photothermal therapy. The conjugation of FA provided FA/PEI/O-MCN with the targeting ability to cancer cells with over-expressed folate receptor. Moreover, DOX-loaded FA/PEI/O-MCN under NIR laser irradiation exhibited the highest cytotoxicity to HeLa cells, comparing with chemotherapy or photothermal treatment alone. Taken together, the mesoporous carbon nanocarrier has demonstrated the promising feasibility of the targeted chemo-photothermal therapy for cancer cells by the combination of the receptor-specific targeting, the NIR-induced hyperthermia and the drug delivery.

Acknowledgements

The financial supports from the National Natural Science Foundation of China (Nos. 21175134, 21375125) and the Creative Research Group Project of National Natural Science Foundation of China (21321064) are greatly acknowledged.

References

1. Huang, X.; Jain, P. K.; El-Sayed, I. H.; El-Sayed, M. A., Determination of the Minimum Temperature Required for Selective Photothermal Destruction of Cancer Cells with the Use of Immunotargeted Gold Nanoparticles. *Photochemistry and Photobiology* **2006,** *82* (2), 412-417.
2. NIG, K. K. È., Multiphoton microscopy in life sciences. *Journal of Microscopy* **2000,** *200* (2), 83-104.
3. Wang, Y.; Black, K. C. L.; Luehmann, H.; Li, W.; Zhang, Y.; Cai, X.; Wan, D.; Liu, S.-Y.; Li, M.; Kim, P.; Li, Z.-Y.; Wang, L. V.; Liu, Y.; Xia, Y., Comparison Study of Gold Nanohexapods, Nanorods, and Nanocages for Photothermal Cancer Treatment. *ACS Nano* **2013,** *7* (3), 2068-2077.
4. Chen, J.; Wang, D.; Xi, J.; Au, L.; Siekkinen, A.; Warsen, A.; Li, Z.-Y.; Zhang, H.; Xia, Y.; Li, X., Immuno gold nanocages with tailored optical properties for targeted photothermal destruction of cancer cells. *Nano Letters* **2007,** *7* (5), 1318-1322.
5. Chen, J.; Glaus, C.; Laforest, R.; Zhang, Q.; Yang, M.; Gidding, M.; Welch, M. J.; Xia, Y., Gold Nanocages as Photothermal Transducers for Cancer Treatment. *Small* **2010,** *6* (7), 811-817.
6. Lal, S.; Clare, S. E.; Halas, N. J., Nanoshell-Enabled Photothermal Cancer Therapy: Impending Clinical Impact. *Accounts of Chemical Research* **2008,** *41* (12), 1842-1851.
7. Yuan, H.; Khoury, C. G.; Wilson, C. M.; Grant, G. A.; Bennett, A. J.; Vo-Dinh, T., In vivo particle tracking and photothermal ablation using plasmon-resonant gold nanostars. *Nanomedicine: Nanotechnology, Biology and Medicine* **2012,** *8* (8), 1355-1363.
8. Huang, X.; Tang, S.; Mu, X.; Dai, Y.; Chen, G.; Zhou, Z.; Ruan, F.; Yang, Z.; Zheng, N., Free standing palladium nanosheets with plasmonic and catalytic properties. *Nature Nanotechnology* **2011,** *6* (1), 28-32.
9. Kam, N. W. S.; O'Connell, M.; Wisdom, J. A.; Dai, H. J., Carbon nanotubes as multifunctional biological transporters and near-infrared agents for selective cancer cell destruction. *Proceedings of the National Academy of Sciences of the United States of America* **2005,** *102* (33), 11600-11605.
10. Chakravarty, P.; Marches, R.; Zimmerman, N. S.; Swafford, A. D. E.; Bajaj, P.; Musselman, I. H.; Pantano, P.; Draper, R. K.; Vitetta, E. S., Thermal ablation of tumor cells with antibody-functionalized single-walled carbon nanotubes. *Proceedings of the National Academy of Sciences* **2008,** *105* (25), 8697-8702.
11. Fisher, J. W.; Sarkar, S.; Buchanan, C. F.; Szot, C. S.; Whitney, J.; Hatcher, H. C.; Torti, S. V.; Rylander, C. G.; Rylander, M. N., Photothermal Response of Human and Murine Cancer Cells to Multiwalled Carbon Nanotubes after Laser Irradiation. *Cancer Research* **2010,** *70* (23), 9855-9864.
12. Miyako, E.; Nagata, H.; Hirano, K.; Makita, Y.; Nakayama, K.-i.; Hirotsu, T., Near-infrared laser-triggered carbon nanohorns for selective elimination of microbes. *Nanotechnology* **2007,** *18* (47), 475103.
13. Miyako, E.; Deguchi, T.; Nakajima, Y.; Yudasaka, M.; Hagihara, Y.; Horie, M.; Shichiri, M.; Higuchi, Y.; Yamashita, F.; Hashida, M.; Shigeri, Y.; Yoshida, Y.; Iijima, S., Photothermic regulation of gene expression triggered by laser-induced carbon nanohorns. *Proceedings of the National Academy of*

Sciences **2012,** *109* (19), 7523-7528.

14. Yang, K.; Zhang, S.; Zhang, G.; Sun, X.; Lee, S.-T.; Liu, Z., Graphene in Mice: Ultrahigh In Vivo Tumor Uptake and Efficient Photothermal Therapy. *Nano Letters* **2010,** *10* (9), 3318-3323.

15. Seo, W. S.; Lee, J. H.; Sun, X.; Suzuki, Y.; Mann, D.; Liu, Z.; Terashima, M.; Yang, P. C.; McConnell, M. V.; Nishimura, D. G.; Dai, H., FeCo/graphitic-shell nanocrystals as advanced magnetic-resonance-imaging and near-infrared agents. *Nature Materials* **2006,** *5* (12), 971-976.

16. Sherlock, S. P.; Tabakman, S. M.; Xie, L.; Dai, H., Photothermally Enhanced Drug Delivery by Ultrasmall Multifunctional FeCo/Graphitic Shell Nanocrystals. *ACS Nano* **2011,** *5* (2), 1505-1512.

17. Wang, H.; Zhao, Y.-L.; Nie, G.-J., Multifunctional nanoparticle systems for combined chemoand photothermal cancer therapy. *Frontiers of Materials Science* **2013,** *7* (2), 118-128.

18. Hauck, T. S.; Jennings, T. L.; Yatsenko, T.; Kumaradas, J. C.; Chan, W. C. W., Enhancing the Toxicity of Cancer Chemotherapeutics with Gold Nanorod Hyperthermia. *Advanced Materials* **2008,** *20* (20), 3832-3838.

19. Li, R.; Wu, R. a.; Zhao, L.; Wu, M.; Yang, L.; Zou, H., P-Glycoprotein Antibody Functionalized Carbon Nanotube Overcomes the Multidrug Resistance of Human Leukemia Cells. *ACS Nano* **2010,** *4* (3), 1399-1408.

20. Zhang, W.; Guo, Z.; Huang, D.; Liu, Z.; Guo, X.; Zhong, H., Synergistic effect of chemo-photothermal therapy using PEGylated graphene oxide. *Biomaterials* **2011,** *32* (33), 8555-8561.

21. Qin, X. C.; Guo, Z. Y.; Liu, Z. M.; Zhang, W.; Wan, M. M.; Yang, B. W., Folic acid-conjugated graphene oxide for cancer targeted chemo-photothermal therapy. *Journal of Photochemistry and Photobiology B: Biology* **2013,** *120*, 156-162.

22. Liu, Z.; Robinson, J. T.; Sun, X.; Dai, H., PEGylated nanographene oxide for delivery of water-insoluble cancer drugs. *Journal of the American Chemical Society* **2008,** *130* (33), 10876-10877.

23. Wajid, A. S.; Das, S.; Irin, F.; Ahmed, H. S. T.; Shelburne, J. L.; Parviz, D.; Fullerton, R. J.; Jankowski, A. F.; Hedden, R. C.; Green, M. J., Polymer-stabilized graphene dispersions at high concentrations in organic solvents for composite production. *Carbon* **2012,** *50* (2), 526-534.

24. Chen, H.; Zhang, X.; Dai, S.; Ma, Y.; Cui, S.; Achilefus, S.; Gu, Y., Multifunctional Gold Nanostar Conjugates for Tumor Imaging and Combined Photothermal and Chemo-therapy. *Theranostics* **2013,** *3* (9), 633-649.

25. Chen, Y.-S.; Frey, W.; Kim, S.; Homan, K.; Kruizinga, P.; Sokolov, K.; Emelianov, S., Enhanced thermal stability of silica-coated gold nanorods for photoacoustic imaging and image-guided therapy. *Optics Express* **2010,** *18* (9), 8867-8877.

26. Yang, X.; Liu, Z.; Li, Z.; Pu, F.; Ren, J.; Qu, X., Near-Infrared-Controlled, Targeted Hydrophobic Drug-Delivery System for Synergistic Cancer Therapy. *Chemistry - A European Journal* **2013,** *19* (31), 10388-10394.

27. Tang, H.; Shen, S.; Guo, J.; Chang, B.; Jiang, X.; Yang, W., Gold nanorods@mSiO_2 with a smart polymer shell responsive to heat/near-infrared light for chemo-photothermal therapy. *Journal of Materials Chemistry* **2012,** *22* (31), 16095-16103.

28. Shen, S.; Tang, H.; Zhang, X.; Ren, J.; Pang, Z.; Wang, D.; Gao, H.; Qian, Y.; Jiang, X.; Yang, W., Targeting mesoporous silica-encapsulated gold nanorods for chemo-photothermal therapy with near-infrared radiation. *Biomaterials* **2013,** *34* (12), 3150-3158.

29. Wang, D.-W.; Zhu, X.-M.; Lee, S.-F.; Chan, H.-M.; Li, H.-W.; Kong, S. K.; Yu, J. C.; Cheng, C. H. K.; Wang, Y.-X. J.; Leung, K. C.-F., Folate-conjugated Fe_3O_4@SiO_2@gold nanorods@mesoporous SiO_2

hybrid nanomaterial: a theranostic agent for magnetic resonance imaging and photothermal therapy. *Journal of Materials Chemistry B* **2013,** *1* (23), 2934-2942.

30. Yang, J. P.; Shen, D. K.; Zhou, L.; Li, W.; Li, X. M.; Yao, C.; Wang, R.; El-Toni, A. M.; Zhang, F.; Zhao, D. Y., Spatially Confined Fabrication of Core-Shell Gold Nanocages@Mesoporous Silica for Near-Infrared Controlled Photothermal Drug Release. *Chemistry of Materials* **2013,** *25* (15), 3030-3037.

31. Fang, W. J.; Tang, S. H.; Liu, P. X.; Fang, X. L.; Gong, J. W.; Zheng, N. F., Pd Nanosheet-Covered Hollow Mesoporous Silica Nanoparticles as a Platform for the Chemo-Photothermal Treatment of Cancer Cells. *Small* **2012,** *8* (24), 3816-3822.

32. Li, H.; Tan, L.-L.; Jia, P.; Li, Q.-L.; Sun, Y.-L.; Zhang, J.; Ning, Y.-Q.; Yu, J.; Yang, Y.-W., Near-infrared light-responsive supramolecular nanovalve based on mesoporous silica-coated gold nanorods. *Chemical Science* **2014,** *5* (7), 2804-2808.

33. Qin, H.; Gao, P.; Wang, F.; Zhao, L.; Zhu, J.; Wang, A.; Zhang, T.; Wu, R. a.; Zou, H., Highly Efficient Extraction of Serum Peptides by Ordered Mesoporous Carbon. *Angewandte Chemie International Edition* **2011,** *50* (51), 12218-12221.

34. Qin, H.; Zhao, L.; Li, R.; Wu, R. a.; Zou, H., Size-Selective Enrichment of N-Linked Glycans Using Highly Ordered Mesoporous Carbon Material and Detection by MALDI-TOF MS. *Analytical Chemistry* **2011,** *83* (20), 7721-7728.

35. Gu, J.; Su, S.; Li, Y.; He, Q.; Shi, J., Hydrophilic mesoporous carbon nanoparticles as carriers for sustained release of hydrophobic anti-cancer drugs. *Chemical Communications* **2011,** *47* (7), 2101-2103.

36. Kim, T.-W.; Chung, P.-W.; Slowing, I. I.; Tsunoda, M.; Yeung, E. S.; Lin, V. S. Y., Structurally Ordered Mesoporous Carbon Nanoparticles as Transmembrane Delivery Vehicle in Human Cancer Cells. *Nano Letters* **2008,** *8* (11), 3724-3727.

37. Fang, Y.; Gu, D.; Zou, Y.; Wu, Z.; Li, F.; Che, R.; Deng, Y.; Tu, B.; Zhao, D., A Low-Concentration Hydrothermal Synthesis of Biocompatible Ordered Mesoporous Carbon Nanospheres with Tunable and Uniform Size. *Angewandte Chemie International Edition* **2010,** *49* (43), 7987-7991.

38. Zhu, J.; Liao, L.; Bian, X.; Kong, J.; Yang, P.; Liu, B., pH-Controlled Delivery of Doxorubicin to Cancer Cells, Based on Small Mesoporous Carbon Nanospheres. *Small* **2012,** *8* (17), 2715-2720.

39. Zhu, J.; Liao, L.; Zhu, L.; Kong, J.; Liu, B., Folate Functionalized Mesoporous Carbon Nanospheres as Nanocarrier for Targetted Delivery and Controlled Release of Doxorubicin to HeLa Cells. *Acta Chimica Sinica* **2013,** *71* (1), 69-74.

40. Karavasili, C.; Amanatiadou, E. P.; Sygellou, L.; Giasafaki, D. K.; Steriotis, T. A.; Charalambopoulou, G. C.; Vizirianakis, I. S.; Fatouros, D. G., Development of new drug delivery system based on ordered mesoporous carbons: characterisation and cytocompatibility studies. *Journal of Materials Chemistry B* **2013,** *1* (25), 3167-3174.

41. Chan, S. Y.; Empig, C. J.; Welte, F. J.; Speck, R. F.; Schmaljohn, A.; Kreisberg, J. F.; Goldsmith, M. A., Folate receptor-alpha is a cofactor for cellular entry by Marburg and Ebola viruses. *Cell* **2001,** *106* (1), 117-126.

42. Shen, J.; Hu, Y.; Shi, M.; Lu, X.; Qin, C.; Li, C.; Ye, M., Fast and Facile Preparation of Graphene Oxide and Reduced Graphene Oxide Nanoplatelets. *Chemistry of Materials* **2009,** *21* (15), 3514-3520.

43. Bourlinos, A. B.; Georgakilas, V.; Zboril, R.; Steriotis, T. A.; Stubos, A. K.; Trapalis, C., Aqueous-phase exfoliation of graphite in the presence of polyvinylpyrrolidone for the production of water-soluble graphenes. *Solid State Communications* **2009,** *149* (47-48), 2172-2176.

44. Datsyuk, V.; Kalyva, M.; Papagelis, K.; Parthenios, J.; Tasis, D.; Siokou, A.; Kallitsis, I.; Galiotis, C., Chemical oxidation of multiwalled carbon nanotubes. *Carbon* **2008,** *46* (6), 833-840.

45. Azizi, A.; Khosla, T.; Mitchell, B. S.; Alem, N.; Pesika, N. S., Tuning Carbon Content and Morphology of FeCo/Graphitic Carbon Core-Shell Nanoparticles using a Salt-Matrix-Assisted CVD Process. *Particle & Particle Systems Characterization* **2013**, 31(4), 474-480.

46. Wu, Z.; Webley, P. A.; Zhao, D., Comprehensive Study of Pore Evolution, Mesostructural Stability, and Simultaneous Surface Functionalization of Ordered Mesoporous Carbon (FDU-15) by Wet Oxidation as a Promising Adsorbent. *Langmuir* **2010,** *26* (12), 10277-10286.

47. Jia, Y. F.; Thomas, K. M., Adsorption of cadmium ions on oxygen surface sites in activated carbon. *Langmuir* **2000,** *16* (3), 1114-1122.

48. Wang, Y.; Shi, W.; Song, W.; Wang, L.; Liu, X.; Chen, J.; Huang, R., Tumor cell targeted delivery by specific peptide-modified mesoporous silica nanoparticles. *Journal of Materials Chemistry* **2012,** *22* (29), 14608-14616.

49. Song, Y.; Shi, W.; Chen, W.; Li, X.; Ma, H., Fluorescent carbon nanodots conjugated with folic acid for distinguishing folate-receptor-positive cancer cells from normal cells. *Journal of Materials Chemistry* **2012,** *22* (25), 12568-12573.

50. Oh, J.-M.; Choi, S.-J.; Lee, G.-E.; Han, S.-H.; Choy, J.-H., Inorganic Drug-Delivery Nanovehicle Conjugated with Cancer-Cell-Specific Ligand. *Advanced Functional Materials* **2009,** *19* (10), 1617-1624.

51. Cataldo, F., An Investigation on the Optical Properties of Carbon Black, Fullerite, and Other Carbonaceous Materials in Relation to the Spectrum of Interstellar Extinction of Light. *Fullerenes, Nanotubes and Carbon Nanostructures* **2002,** *10* (2), 155-170.

52. Robinson, J. T.; Tabakman, S. M.; Liang, Y.; Wang, H.; Sanchez Casalongue, H.; Vinh, D.; Dai, H., Ultrasmall Reduced Graphene Oxide with High Near-Infrared Absorbance for Photothermal Therapy. *Journal of the American Chemical Society* **2011,** *133* (17), 6825-6831.

53. Acik, M.; Lee, G.; Mattevi, C.; Chhowalla, M.; Cho, K.; Chabal, Y. J., Unusual infrared-absorption mechanism in thermally reduced graphene oxide. *Nature Materials* **2010,** *9* (10), 840-845.

54. Liu, Z.; Sun, X.; Nakayama-Ratchford, N.; Dai, H., Supramolecular chemistry on water-soluble carbon nanotubes for drug loading and delivery. *ACS Nano* **2007,** *1* (1), 50-56.

55. Yang, X.; Zhang, X.; Liu, Z.; Ma, Y.; Huang, Y.; Chen, Y., High-Efficiency Loading and Controlled Release of Doxorubicin Hydrochloride on Graphene Oxide. *Journal of Physical Chemistry C* **2008,** *112* (45), 17554-17558.

56. Zhang, Z.; Wang, L.; Wang, J.; Jiang, X.; Li, X.; Hu, Z.; Ji, Y.; Wu, X.; Chen, C., Mesoporous Silica-Coated Gold Nanorods as a Light-Mediated Multifunctional Theranostic Platform for Cancer Treatment. *Advanced Materials* **2012,** *24* (11), 1418-1423.

57. Rosenholm, J. M.; Meinander, A.; Peuhu, E.; Niemi, R.; Eriksson, J. E.; Sahlgren, C.; Linden, M., Targeting of Porous Hybrid Silica Nanoparticles to Cancer Cells. *ACS Nano* **2009,** *3* (1), 197-206.

58. Shi Kam, N. W., Carbon nanotubes as multifunctional biological transporters and near-infrared agents for selective cancer cell destruction. *Proceedings of the National Academy of Sciences* **2005,** *102* (33), 11600-11605.

Figure Captions:

Figure 1. Schematic illustration of the preparation of FA/PEI/O-MCN and the chemo-photothermal targeted therapy based on the DOX-loaded FA/PEI/O-MCN.

Figure 2. (A) TEM images of O-MCN (1), PEI/O-MCN (2) and FA/PEI/O-MCN (3), the scale bar is 100 nm; (B) Particle diameter distribution of FA/PEI/O-MCN; (C) Raman spectra (excitation at 514 nm) with the G and D bands of graphitic carbon. (D) N_2 adsorption–desorption isotherm and pore size distribution (inset) curves of O-MCN and FA/PEI/O-MCN.

Figure 3. (A) The FT-IR spectra of MCN (1), O-MCN (2), PEI/O-MCN (3) and FA/PEI/O-MCN (4); (B) UV-Vis-NIR spectra of PEI/O-MCN, FA/PEI/O-MCN and FA.

Figure 4. Zeta potentials of O-MCN, PEI/O-MCN and FA/PEI/O-MCN in PBS. Error bars were based on triplet samples.

Figure 5. (A) Photothermal heating curves of FA/PEI/O-MCN at various concentrations with NIR laser irradiation; (B) Temperature changes with FA/PEI/O-MCN and rGO_{pvp} at various concentrations under NIR laser irradiation (t=2.5 min) and UV-Vis-NIR spectra (inset) of FA/PEI/O-MCN and rGO_{pvp} at the same concentrtion of 50 μg/mL. Error bars were based on triplet samples.

Figure 6. (A) The loading capacity of DOX on O-MCN and FA/PEI/O-MCN at different pH values; (B) NIR-triggered release of DOX at different pH values. The inset shows the release profile of DOX at acidic condition (pH 5.5) in the absence and presence of NIR laser. Error bars were based on triplet samples.

Figure 7. Cytotoxicity detection with CCK8 assay (A) and LDH activity assay (B) for HeLa cells treated with different concentrations of FA/PEI/O-MCN for the indicated times.

Figure 8. (A) Analysis of cellular uptake of DOX-loaded nanocomposites by flow cytometry (from left to right: control, DOX-loaded PEI/O-MCN, DOX-loaded FA/PEI/O-MCN); (B) Cellular uptake of FA/PEI/O-MCN by optical microscope. HeLa cells were incubated with 25 μg/mL FA/PEI/O-MCN for 12 h in folate medium (1, 2) and folate-free medium (3,4); Scale bars represent 50 μm; (C) Cytotoxicity of

FA/PEI/O-MCN on HeLa cells incubated at different culture media with and without NIR laser irradiation (15 W/cm^2 for 5 min per treatment, three treatments).

Figure 9. (A) The cell viability of HeLa cells treated with FA/PEI/O-MCN, NIR + FA/PEI/O-MCN, DOX-loaded FA/PEI/O-MCN and NIR+DOX-loaded FA/PEI/O-MCN, NIR represents irradiated by 808 nm laser with power of 15W/cm^2 for 5 min, three treatments; (B) Temperature changes of HeLa cells incubated with various concentrations of FA/PEI/O-MCN after exposed to 808 nm laser for 5 min.

Figure 1.

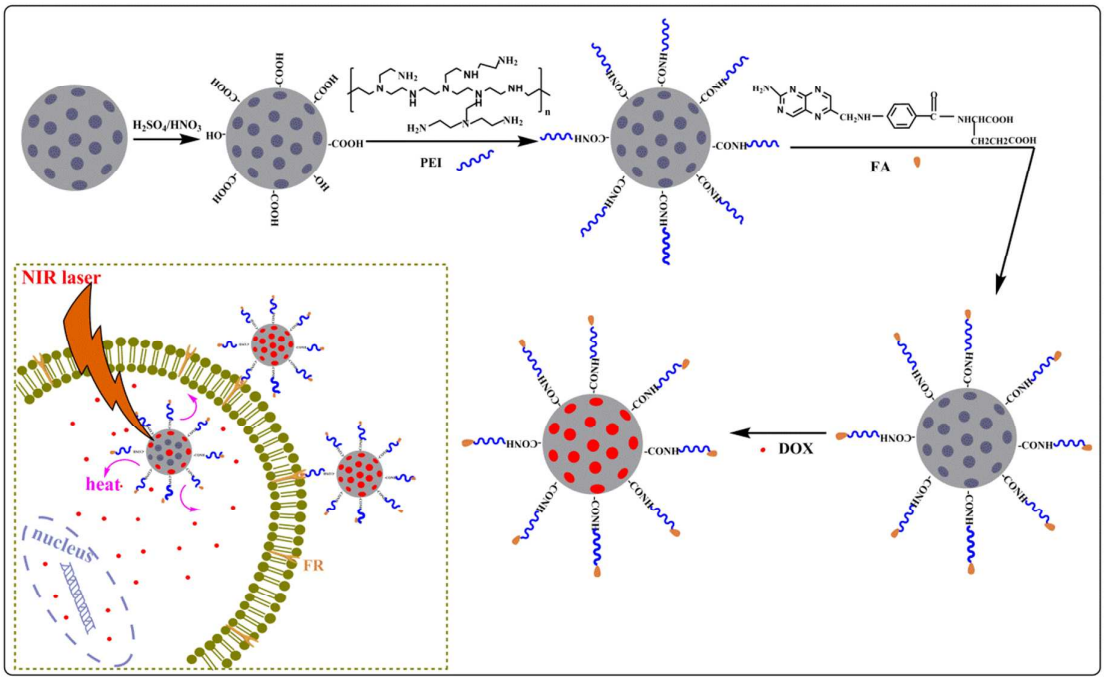

Figure 2.

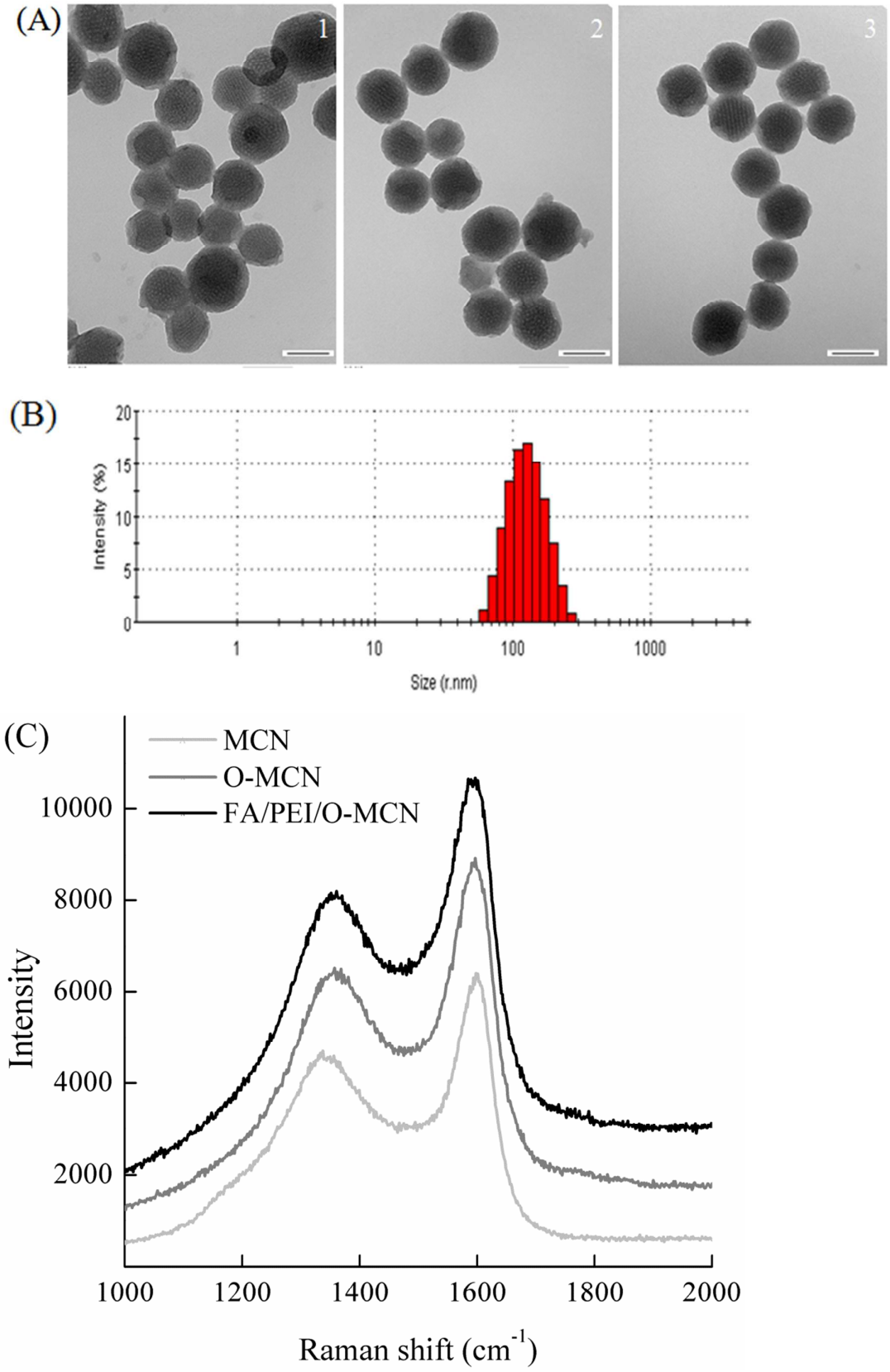

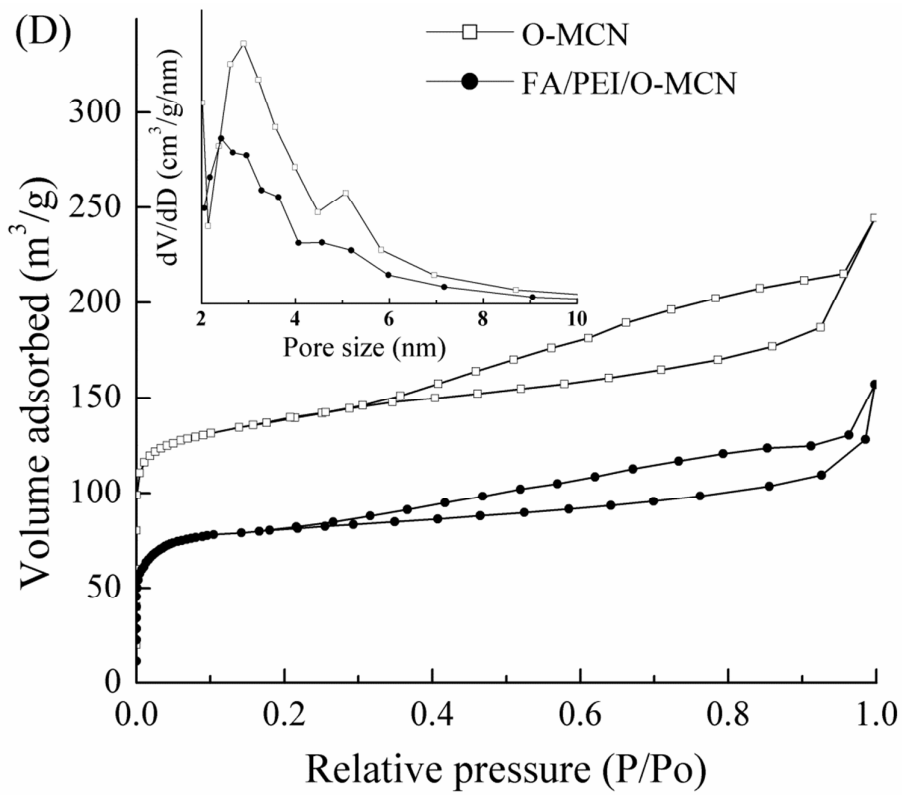

Figure 3.

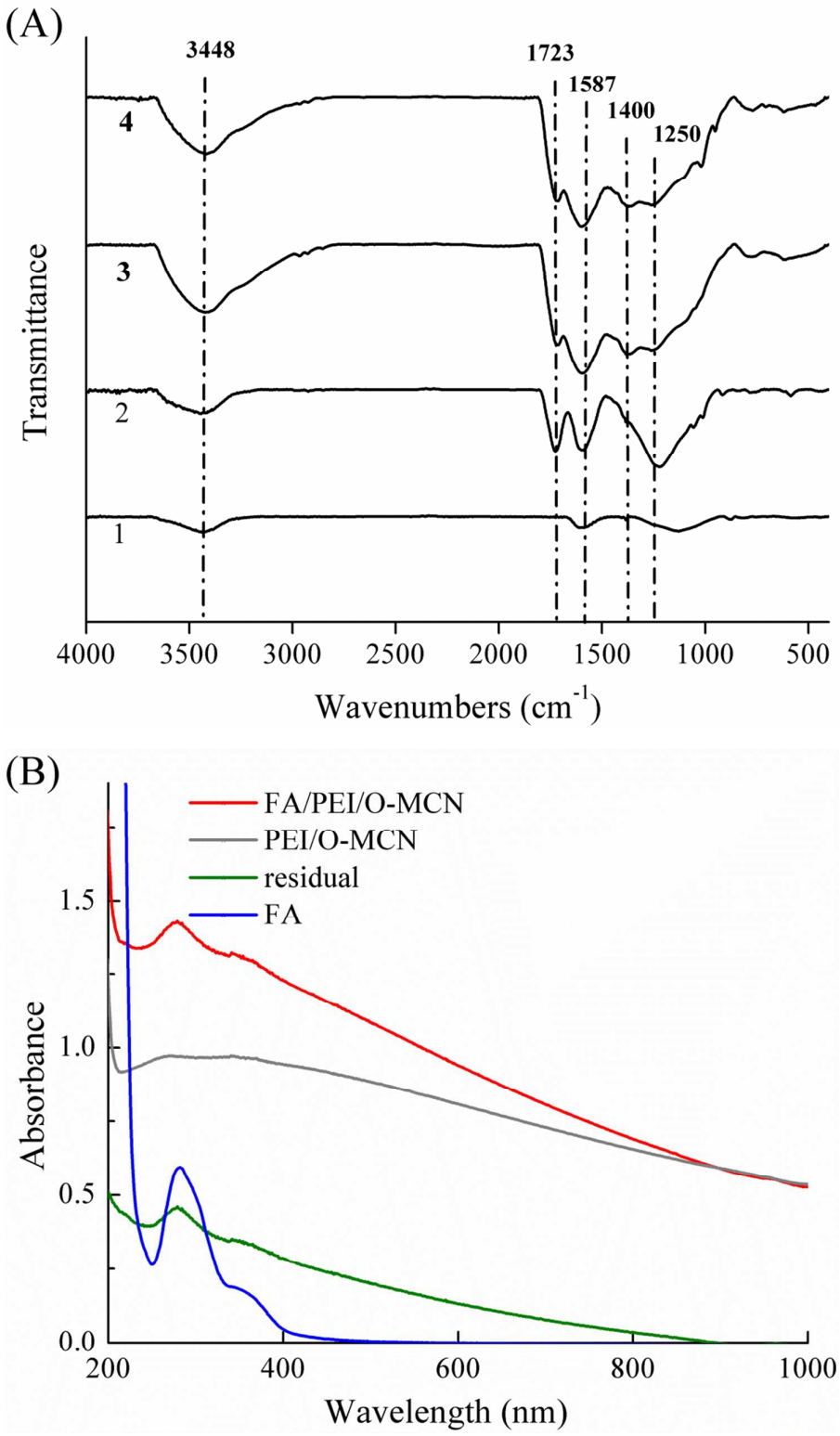

Figure 4.

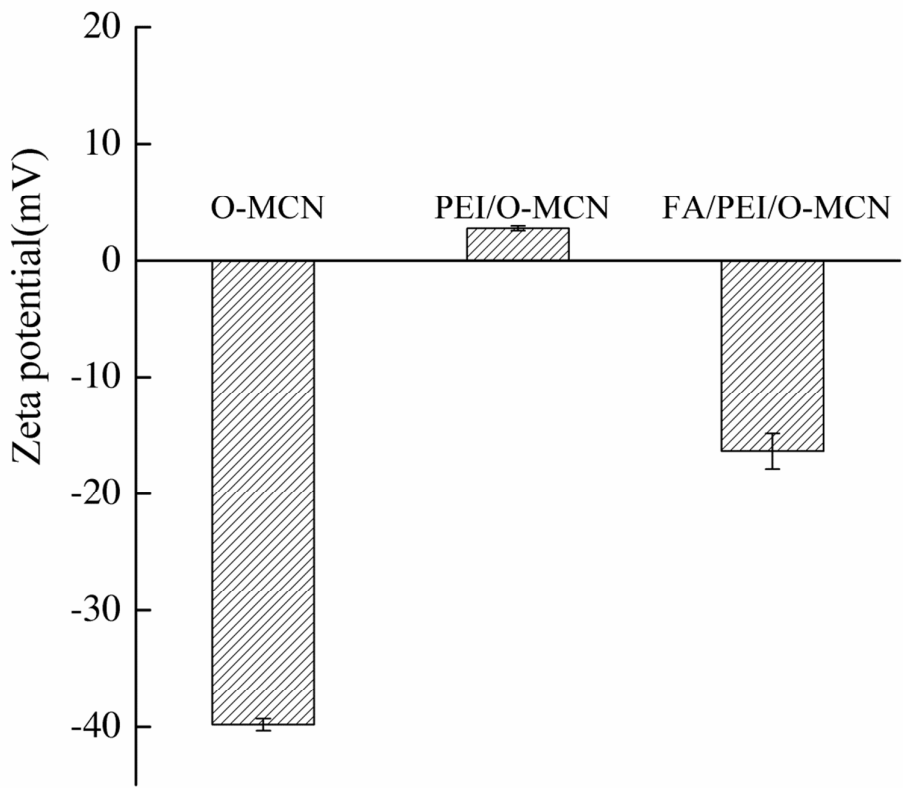

Figure 5.

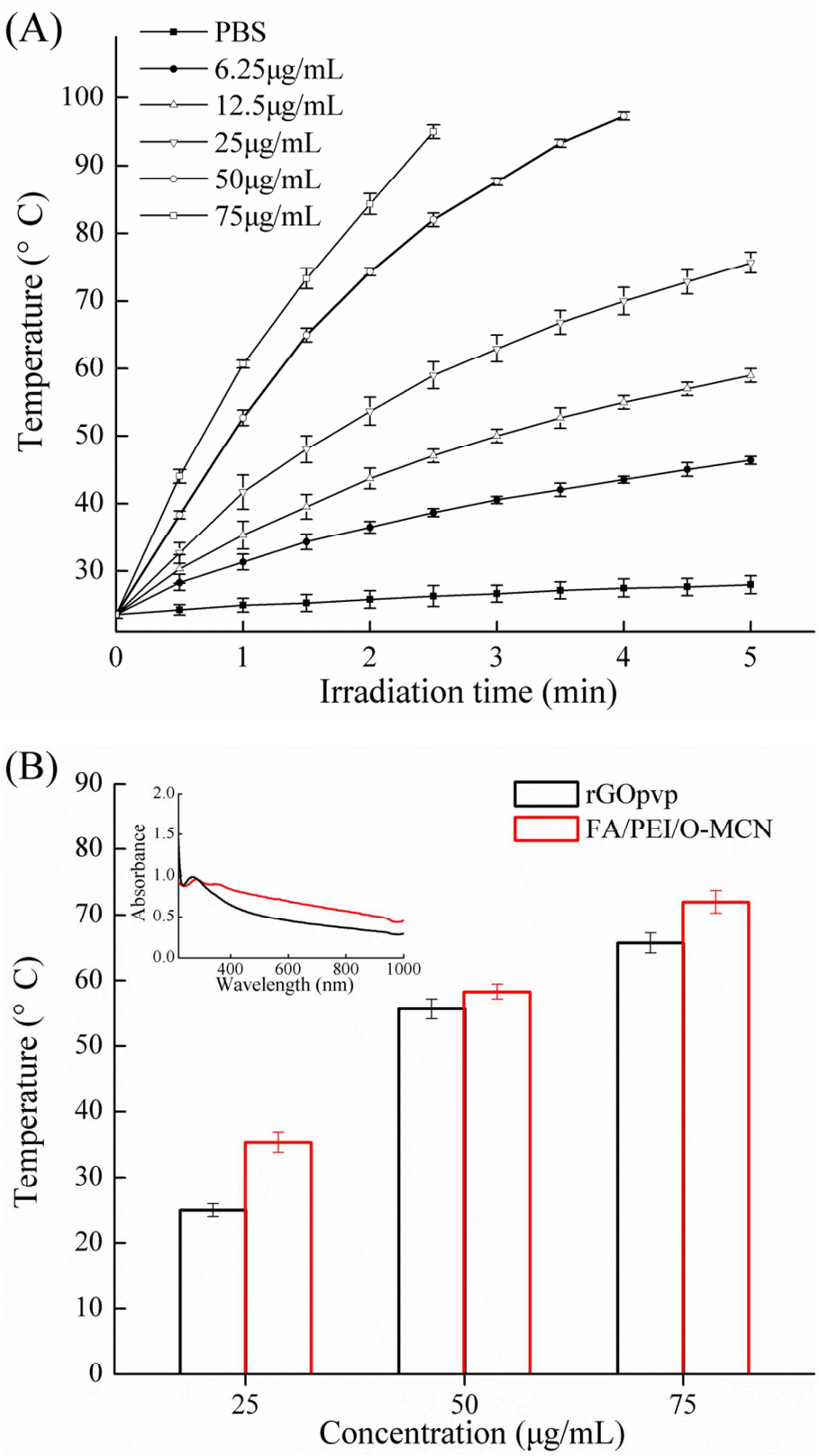

Figure 6.

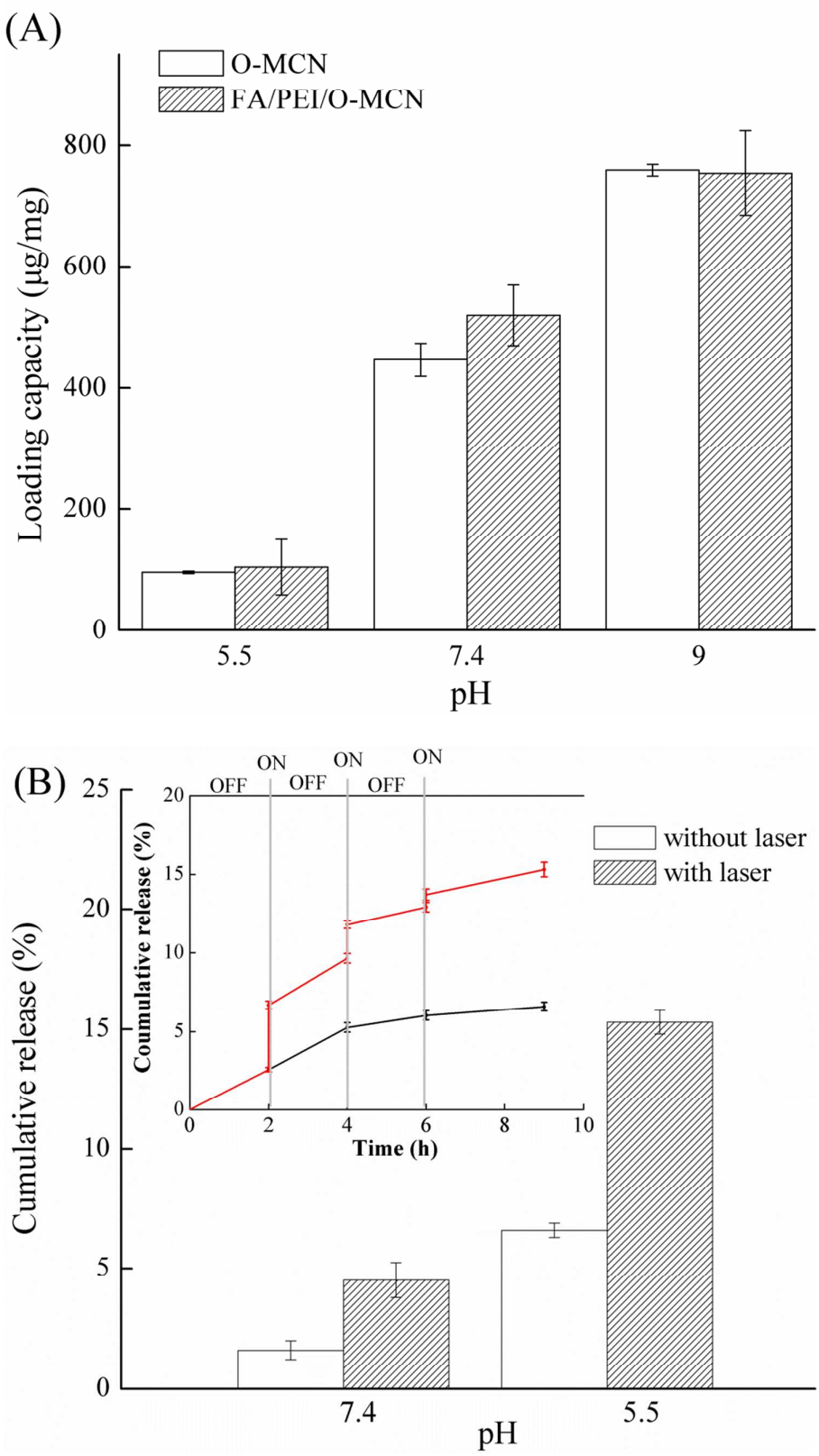

Figure 7.

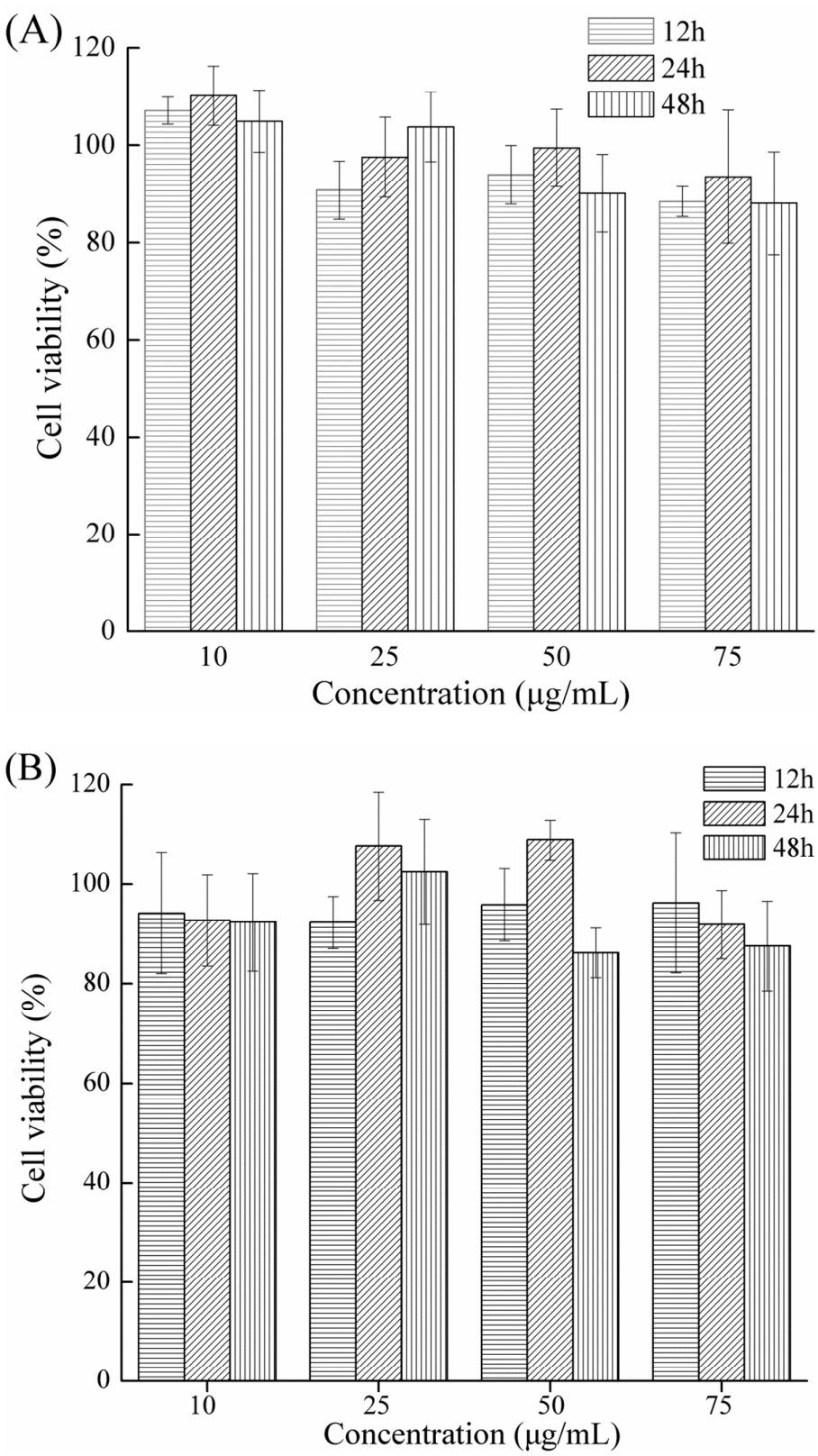

Figure 8.

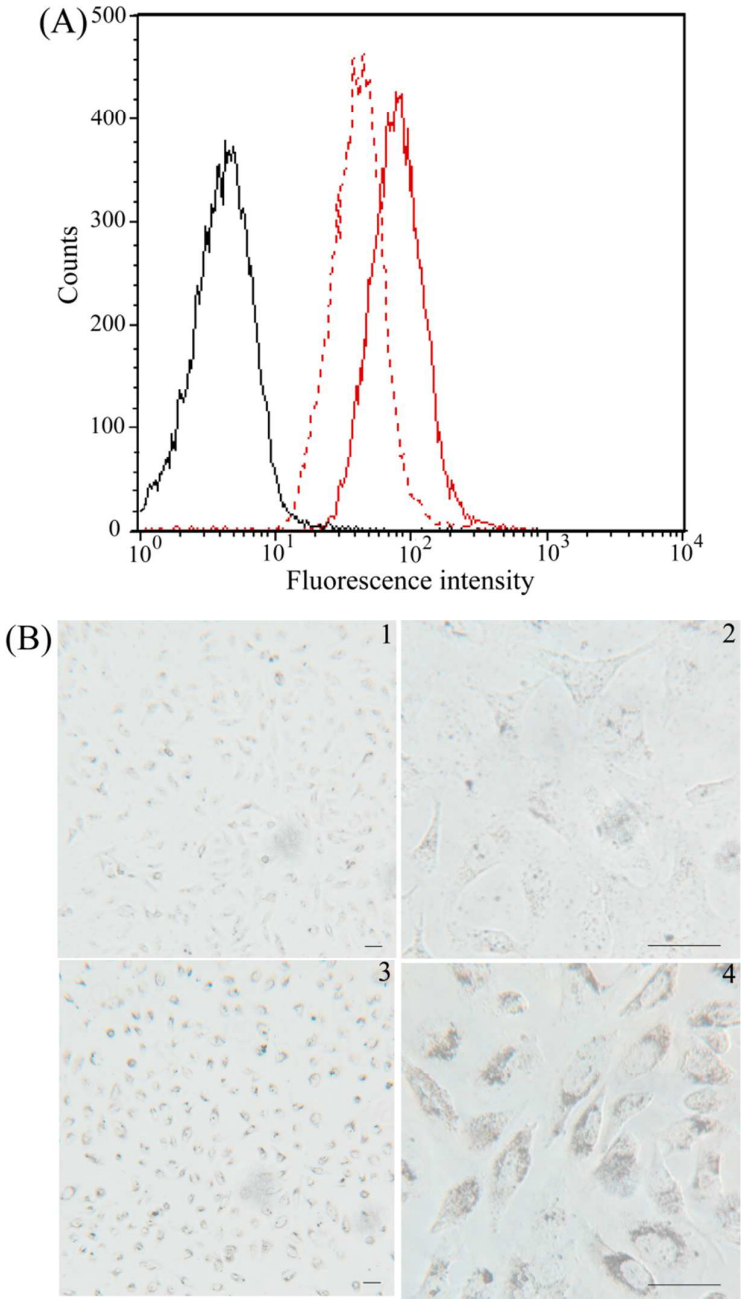

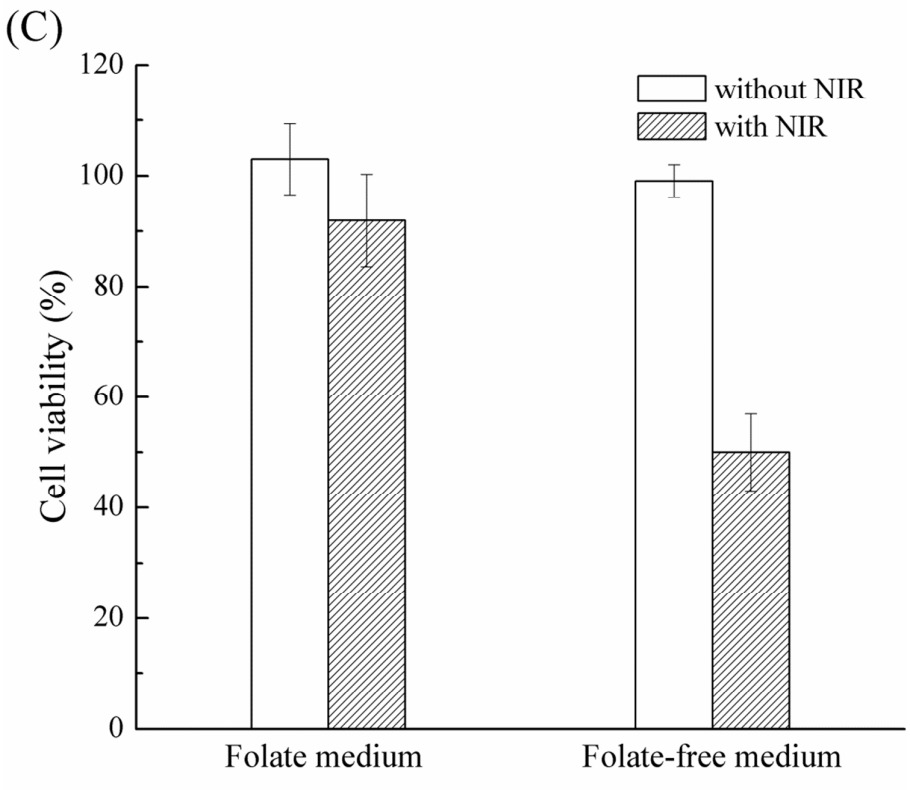

Figure 9.